Energetics, structure, and charge distribution of reduced and oxidized *n*-pyrrole oligomers: A density functional approach

Yafei Dai and Estela Blaisten-Barojas[a)]
Computational Materials Science Center and Department of Computational and Data Sciences, George Mason University, Fairfax, Virginia 22030, USA

(Received 5 June 2008; accepted 15 September 2008; published online 27 October 2008)

Polypyrrole is a conjugated polymer prototype of conducting polymers. The energetically preferred spatial conformation of *n*-pyrrole oligomers ($n=1-24$) in both the reduced and oxidized phases is obtained and analyzed in this paper within the hybrid density functional theory. Binding energies, gap energies, radius of gyration, end-to-end distance, and vibrational frequencies are reported as functions of oligomer length. Reduced *n*-pyrrole are bent chains for all sizes showing a dramatic departure from planarity. Vibrational spectra of *n*-pyrrole oligomers indicate the presence of two fairly size-insensitive frequency regions, which increase in intensity with increasing oligomer size. Several oxidation levels were analyzed for *n*-pyrrole through the distribution of the carbon-carbon bond orders and single/double bond lengths. It is shown that the oxidation level is directly related to the way positive charge localizes along the *n*-pyrrole oligomer chain. If charge/$n<1/3$, the oligomers are bent and charge is delocalized; if charge/$n\geqslant 1/3$, the oligomers are planar and charge notoriously localizes in *n*/charge regions along the backbone. Calculations with electronegative dopants show that charge localizes in the neighborhood of the dopant. It is demonstrated that one localized state in the gap between the highest occupied and lowest-unoccupied states appears for every $+2e$ in the oxidation level. The band structure of infinite reduced polypyrrole gives a band gap energy in excellent agreement with experiment. The evolution of the band gap and the charge-localized band as a function of polypyrrole oxidation level is reported. © *2008 American Institute of Physics*. [DOI: 10.1063/1.2996297]

I. INTRODUCTION

Polypyrrole (PPy) is a prototypical conducting polymer. Because of its strong electrical and optical anisotropies, PPy is a good candidate for photonic devices. The discovery of photoinduced charge transfer between polymers and their environment (either a substrate or a solid solvent) has led to efficient heterojunctions of polymer/substrate with important applications in solar cells and chemical detectors. However, the lack of knowledge about the recombination dynamics and polaron mobility is a bottleneck to improve any device efficiency. By electrochemical polymerization, PPy is synthesized in two different phases: reduced when the polymer is electrically neutral and oxidized when the polymer is positively charged, having transferred electrons to the oxidizing agent.[1,2]

Theoretical studies of PPy have extensively used semiempirical and Hartree–Fock (HF) methods. For example, the ultraviolet photoemission and optical absorption spectra for pyrrole (Py) and PPy were analyzed using a spectroscopically parametrized complete neglect of differential overlap method;[3] the vibrational spectra of PPy was studied at the modified neglect of differential overlap level,[4] and the band structure of PPy within the intermediate neglect of differential overlap approximation was published.[5] At the Hartree Fock level, there have been several studies as well: the ground states of Py, 2-Py, and PPy,[6] the effect of charge-transfer doping on the geometry of PPy,[7–9] the energetics of Py dimers as a function of the torsion angle,[10] and structure coupled with vibrational spectra.[11,12] More recently, density functional theory (DFT) calculations of PPy have been undertaken for a variety of studies, for example, studies on the band gap of conducting polymers,[13] electronic and structural properties of oxidized PPy with chlorine dopants,[14] the excited states of the Py monomer and dimer,[15] and their vibrational frequencies.[16] Despite these studies, the positive charge localization mechanism that occurs in oxidized PPy has not been given a proper description at the quantum level.

The purpose of this study is to investigate the energetics of reduced and oxidized *n*-Py oligomers and the positive charge localization as a function of oligomer length (n). Results in these areas are pertinent for studies of polaron and bipolaron formation.[17–19] To that end, the geometrical structures of *n*-Py ($n=1-9,12,15,18,20,24$) and infinite PPy chains were studied in their reduced and oxidized phases within the hybrid DFT framework with large basis sets. This paper is organized as follows: Section II describes the methodology used as well as the results for the Py and bipyrrole molecules. Sec. III describes the geometrical configurations

a)Electronic mail: blaisten@gmu.edu.

TABLE I. IR-active spectrum of anti-*gauche* and syn-*gauche* bipyrrole (str=stretch, i-r=inter-ring, rd=ring deform, ipb=in-plane bend, oopb=out-of-plane bend, oopr=out-of-plane rotation, and ripr=ring in-plane rotation).

Expt.[a]	anti-*gauche*		syn-*gauche*		
(cm^{-1})	(cm^{-1})	I_{IR}	(cm^{-1})	I_{IR}	Assignment
			a		
	3697	9.8	3692	57.4	N—H str
	3286	0.0	3285	0.0	C—H str
	3262	1.3	3268	9.1	C—H str
	3246	0.3	3252	0.25	C—H str
1618	1674	0.0	1671	0.4	C—C i-r str
1479	1523	1.2	1522	10.2	C—C, C—N str
1453	1477	1.6	1457	4.9	C—N, C—C str
1410	1450	0.3	1430	4.8	C—N, C—C str
1303	1345	1.8	1323	7.9	C—C str, N—H ipb
1263	1314	0.0	1287	0.8	CH ipb
1118	1162	1.5	1158	9.0	C—N—C—H ipb
1098	1132	1.8	1127	22.4	H—C=C—H
1029	1071	1.6	1065	29.0	H—C—C—H ipb
960	990	0.2	986	1.3	rd, C—H ipb
880	915	0.3	921	3.4	rd
	444	0.8	394	0.2	ripr
392	392	0.0	359	3.0	Ring ip transl
	902	0.18	910	0.1	C—H oopb
789	819	77.3	847	16.9	C—H oopb
727	736	170.3	738	22.3	C—H oopb
669	671	1.8	704	0.6	Ring def
584	642	49.6	654	30.5	Ring def
	623	107.2	624	31.4	N—H oopb
	121	0.6	122	0.2	Ring oopb
	63	3.6			Ring oopr
			b		
3365	3697	73.2	3691	19.5	N—H str
	3286	10.1	3284	10.7	C—H str
3120	3262	12.8	3268	2.4	C—H str
3100	3247	19.0	3251	15.7	C—H str
1527	1581	39.2	1589	30.4	C=C str
1425	1471	4.6	1485	7.4	N—C=C
1415	1443	13.0	1454	12.3	H—C—C—H
	1431	12.7	1439	1.7	C—C str
1252	1294	9.8	1313	4.9	C—H, N—H ipb
1147	1179	0.2	1173	0.2	Ring breath
1105	1138	55.7	1146	27.8	H—C—C—H, H—C—N—H
	1096	31.9	1091	13.8	C—H, N—H ipb
1034	1064	52.9	1061	36.1	C—H ipb
894	931	12.7	924	12.5	rd
	905	2.7	908	0.1	rd, C—H oopb
	130	2.5	117	1.2	Ring ipr
	902	0.2	903	1.0	C—H oopb
795	835	11.8	835	59.6	C—H oopb
692	736	13.4	736	155.2	C—H oopb
652	706	1.9	675	0.2	C—H, C—C i-r oopb
636	641	5.6	635	1.1	C—H, N—H oopb
448	623	22.7	597	135.6	C—H, N—H oopb
330	351	1.7	433	3.7	Ring oopb

[a]References 11 and 26.

and electronic properties of reduced *n*-Py. Sec. IV and V contain the study of charged *n*-Py without dopants and oxidized *n*-Py with dopants, respectively. Section VI contains the results of infinite PPy. Section VII presents the conclusions of this paper.

II. PYRROLE AND BIPYRROLE

DFT and the hybrid Becke–Perdew–Wang 1991 approach were used throughout this study, which includes local and nonlocal correlation functionals.[20,21] A triple valence ba-

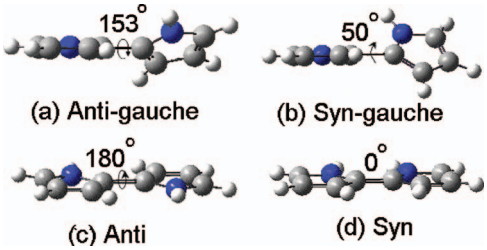

FIG. 1. (Color) Stable bipyrrole isomers showing the torsion angles. [(a) and (b)] Neutral 2-Py; [(c) and (d)] oxidized 2-Py$^+$.

sis set (6-311G) containing 8*s*, 7*p*, and 1*d* Gaussians contracted as (62111111, 3311111, and 3) was adopted in all calculations.[22] The GAUSSIAN 03 package[23] was used throughout. This level of theory reproduces very well the experimental geometry[24] of the neutral Py monomer with a maximum error in geometry variables of 0.8%. The Py molecule is a C_{2v} planar structure with a strong dipole moment of 1.98 D in the direction of the N—H bond and diagonal quadrupole matrix elements of −23.4, −26.5, and −34.1 D Å. The infrared active vibrational frequencies of the two bipyrrole isomers are given in Table I. The agreement of calculated frequencies with experiment[25] is excellent, as indicated by an average ratio of calculated to experimental results of 0.96.

The reduced phase of *n*-Py oligomers and PPy is insulating, charge neutral, and displays the benzenoid alternation of single-double C—C bonds. An alternative realization of the reduced phase is the benzenoid C—C bond alternation attained by electric neutralization of trapped anions (A^-) with solvent cations (C^+). Anions or cations that remain in the polymer matrix during polymerization are called *dopants*. The oxidized phase of PPy (the polymer is positively charged) is the conducting phase displaying conjugated chains with quinoid single-double C—C bond alternation. The change from benzenoid to quinoid structures is promoted by the migration of electrons to the electronegative dopants (A^-). In the oxidized state, *n*-Py and PPy chains are cations.

The geometrical structure of bipyrrole, as well as that of larger oligomers, is modulated the most by the rotational degree of freedom around the inter-ring C—C bond. In principle, reduced 2-Py may have four possible isomers: two puckered structures *anti-gauche* and *syn-gauche* and two planar structures *anti* and *syn*. The oxidized 2-Py may have only two planar isomers: *anti* and *syn*. Energetics along the rotational path yields the stability of rotational isomers as a function of the torsion angle. For neutral 2-Py, the global minimum corresponds to the anti-*gauche* C_2 geometry (torsion angle=153°), which is more stable by 0.033 eV than the planar anti form (180°), 0.122 eV more stable than the syn-*gauche* form (50°) and 0.18 eV more stable than the syn form (0°). Additionally, a normal mode frequency analysis shows that only two neutral isomers are stable, e.g., the anti-*gauche* isomer (C_2 with a torsion angle of 153°) and the syn-*gauche* isomer (C_2 with a torsion angle of 50°) shown in Figs. 1(a) and 1(b). Once relaxed, the binding energy of the anti-*gauche* isomer becomes −119.32 eV, and the syn-*gauche* is 0.07 eV less stable. Therefore, these two neutral isomers can coexist in thermal equilibrium at temperatures of about 700 K. These results are in excellent agreement with MIDI-4 self-consistent field pioneer calculations.[11] For oxidized 2-Py with a $+e$ charge, the two stable isomers are the anti (C_{2h}) and the syn (C_{2v}) planar forms shown in Figs. 1(c)

TABLE II. Vibrational spectrum of anti charged bipyrrole (str=stretch, i-r=inter-ring, rd=ring deform, ipb=in-plane bend, oopb=out-of-plane bend, oopr=out-of-plane rotation, and ripr=ring in-plane rotation).

anti 2-Py$^+$ (C_{2h})							
		a_u			b_u		
a_g (cm^{-1})	b_g (cm^{-1})	(cm^{-1})	I_{IR}	Assignment	(cm^{-1})	I_{IR}	Assignment
3680	952	952	1.8	C—H oopb	3680	178.8	N—H str
3300	880	884	15.6	C—H oopb	3300	8.3	C—H str
3282	787	787	220.1	C—H oopb	3282	9.8	C—H str
3269	687	675	210.4	N—H oopb	3268	0.0	C—H str
1682	672	632	0.0	C—N oopb	1545	100.9	C—H, N—H ipb
1521	577	587	10.7	C—C=C oopb	1502	56.8	C=C, C—N str
1503	302	122	3.5	Ring oopb	1413	369.6	rd
1417		68	4.3	Ring oopr	1400	1.4	C—H, N—H ipb
1393					1224	4.8	rd
1308					1181	6.5	Ring breath
1184					1156	107.3	C—H, N—H ipb
1123					1110	94.4	C—H ipb
1113					1062	13.6	C—H, N—H ipb
969					920	44.0	rd
891					880	5.6	rd
459					155	1.4	ripr
406							

TABLE III. Vibrational spectrum of syn charged bipyrrole (str=stretch, i-r=inter-ring, rd=ring deform, ipb=in-plane bend, oopb=out-of-plane bend, oopr =out-of-plane rotation, ripr=ring in-plane rotation, and ript=ring in-plane translation).

syn 2-Py$^+$ (C_{2v})									
a_1			a_2	b_1			b_2		
(cm^{-1})	I_{IR}	Assignment	(cm^{-1})	(cm^{-1})	I_R	Assignment	(cm^{-1})	I_{IR}	Assignment
3691	156.2	N—H str	954	956	1.5	C—H oopb	3682	0.1	N—H str
3302	1.8	C—H str	883	885	19.3	C—H oopb	3301	6.7	C—H str
3286	4.9	C—H str	785	790	178.7	C—H oopb	3283	5.4	C—H str
3277	0.9	C—H str	681	674	241.5	N—H oopb	3275	0.3	C—H str
1682	6.5	C═C i-r str	591	627	0.6	C—N—C oopb	1544	65.2	C—H, N—H ipb
1514	43.8	N—H ipb	583	577	26.2	C—C—C oopb	1510	31.8	C═C, C—N str
1498	1.6	rd	301	119	1.5	ring oopb	1421	317.3	C—C str
1416	23.9	C—C, N—H ipb	49				1386	8.7	C—H, N—H ipb
1389	13.4	C—H ipb					1296	3.9	C—H ipb
1239	6.2	C—N str					1173	1.0	Ring breath
1169	38.4	H—C—N—H					1156	24.0	H—C—N—H
1126	31.7	H—C—C—C—H					1104	69.0	H—C—C—H
1111	15.5	C—C str					1059	14.6	C—H ipb
966	1.6	rd					912	49.0	rd
902	1.1	rd					875	0.4	rd
407	0.0	ript					456	0.1	ripr
160	0.1	ripr							

and 1(d). The charged anti C_{2h} isomer (6.75 eV above the neutral C_2 anti-*gauche*) is the global minimum, which is lower in energy by 0.144 eV than the charged syn C_{2v} isomer. A high torsional energy barrier of 1.146 eV makes the transition between the two charged isomers not thermally possible.

Table I lists the calculated normal mode IR-active frequencies for the two neutral bipyrrole isomers, and Tables II and III contain similar information for the positively charged 2-Py$^+$ isomers. The results for the neutral isomers are in very good agreement with experiment[11,26] (Table I, columns 1, 2, and 5). It is to be noted that at the time of the experiments, the symmetry assignment given to neutral bipyrrole was D_{2h}, only based on the frequency assignments of infinite chains. Our comparison shows that the agreement between experiment and calculation for anti-*gauche* or syn-*gauche* bipyrrole isomers is excellent. Therefore, the identification of the molecular symmetry through that IR experiment should be C_2. A frequency scaling factor can be defined as the ratio between the calculated and experimental frequencies, which, based on values in Table I, is on average 0.97. Additionally, Tables II and III contain the non-IR active frequencies of the a_g and b_g modes in the case of the anti C_{2h} charged isomer and of the a_2 mode in the case of the syn C_{2v} charged isomer.

III. STRUCTURE AND ENERGETICS OF REDUCED *n*-Py OLIGOMERS

A geometry optimization of the larger reduced *n*-Py was performed for all sizes with *n* up to 24. The search for the structures of lowest energy was conducted for each oligomer size with the following strategy. A multitude of oligomer structures from molecular dynamics trajectories using an in-house potential model[27] were used as initial geometries for the optimization to a minimum of the energy, which was performed with the Berny algorithm and redundant internal coordinates.[28] Because the most stable isomer of neutral bipyrrole is the anti-*gauche* form, only repetitions of this form were optimized for larger *n*-Py oligomers. Combinations of anti-*gauche* with syn-*gauche* forms were not attempted. All geometrical optimizations of the electronic states include the harmonic frequency calculations to ensure finding of minima. Multiple configurations were not minima but rather saddles of different orders, which are not reported in this paper. Some of these unstable geometries were chains with

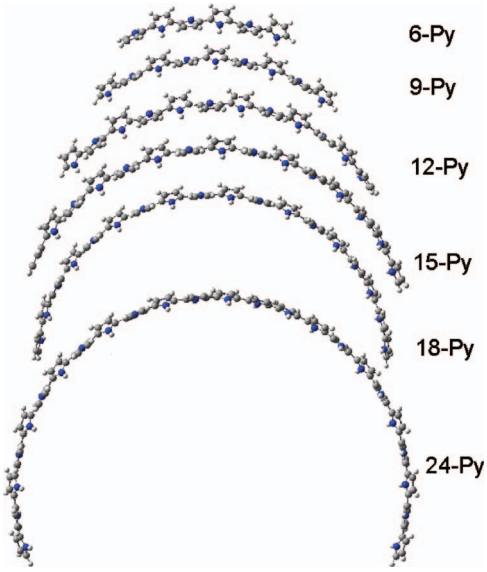

FIG. 2. (Color) Optimized structures for reduced *n*-Py (*n*=6, 9, 12, 15, 18, and 24).

TABLE IV. Binding energies and HOMO-LUMO energy gap for *n*-Py in the reduced phase and *m*+ oxidized phases (*m*=2-6, 8, 10, and 12). Energies are in eV; all energies are referred to the ground state of the neutral oligomer (second row).

	Reduced				Oxidized							
	Singlet		Triplet		q^{2+}	q^{3+}	q^{4+}	q^{5+}	q^{6+}	q^{8+}	q^{10+}	q^{12+}
n-Py	^1E_b	Δ_{HL}	^3E_b	Δ_{HL}	E_b							
1	−62.09	6.87	3.87	3.42	24.03	⋯	⋯	⋯	⋯	⋯	⋯	⋯
2	−119.32	5.21	2.84	3.24	18.72	⋯	⋯	⋯	⋯	⋯	⋯	⋯
3	−176.56	4.46	2.45	2.45	16.50	⋯	⋯	⋯	⋯	⋯	⋯	⋯
4	−233.80	4.07	2.30	2.01	15.20	⋯	⋯	⋯	⋯	⋯	⋯	⋯
5	−291.04	3.84	2.22	1.83	14.34	⋯	⋯	⋯	⋯	⋯	⋯	⋯
6	−348.28	3.69	2.19	1.64	13.73	24.94	39.24	⋯	⋯	⋯	⋯	⋯
9	−519.99	3.46	2.15	1.44	12.60	21.92	33.73	⋯	64.78	⋯	⋯	⋯
12	−691.71	3.36	2.15	1.33	11.93	⋯	30.67	⋯	57.26	92.18	⋯	⋯
15	−863.43	3.31	2.14	1.29	11.48	19.08	28.71	39.62	52.41	⋯	120.95	⋯
18	−1035.14	3.29	2.14	1.28	11.16	⋯	⋯	⋯	49.02	76.71	⋯	150.82

wavy shapes almost degenerate in energy with the ground state. The ground states of the *n*-Py neutral oligomers are singlet electronic states.

The C—C single-double conjugation in *n*-Py is believed to result in a stiff backbone reluctant to bend and twist. Indeed, the picture that most experimentalists have of reduced *n*-Py is that of planar oligomers.[26,29] This belief is a result of semiempirical quantum mechanical approximations such as INDO that are not computer intensive and can be readily calculated in any type of computational platform. Our calculations are based on a better quantum approximation that predicts a different paradigm displayed in Fig. 2. This figure shows the optimized bent configurations of reduced 6-, 9-, 12-, 15-, 18-, and 24-Py. Notice that the torsion angle, as defined for 2-Py, continues to be approximately 153° between neighboring monomers. However, the end-to-end distance and the radius of gyration are substantially different from those in planar chains. This chain bending is one of the reasons why PPy, irrespective of the fabrication process,[1,2,30] tends to form amorphous rather than crystalline arrays of stacked chains.[26] This effect has also an important role in the volume contraction seen experimentally when an oxidized PPy sample is reduced. These bent conformations are in qualitative agreement with those reported recently within density functional calculations with smaller basis sets.[9]

Although the point group of reduced Py is C_{2v}, larger chains present a loss of symmetry; the even-*n*-Py reduced oligomers are C_2 (see Fig. 2) and odd-*n*-Py are C_s. Chains are less symmetric, reflecting the bending of the backbone away from a plane. Binding energies of the ground singlet state ^1E_b, the first excited trimer state ^3E_b, and the highest occupied molecular orbital–lowest unoccupied molecular orbital (HOMO-LUMO) energy gap Δ_{HL} are reported in Table IV (columns 2–5). The binding energy of the triplet state is reported relative to that of the singlet state. The Δ_{HL} for the monomer and dimer are larger than the experimentally reported[31] values of 5.97 and 4.49 eV, respectively. This is to be expected for small molecules as one of the deficiencies of DFT. Figure 3(a) illustrates the binding energy per monomer of singlet states of *n*-Py showing a sharp increase for small chains and a slow asymptotic behavior for large chains toward the limiting energy of an infinite chain of −57.17 eV/monomer. Figure 3(b) is a plot of Δ_{HL} showing a sharp decrease as short oligomers increase the number of monomers. A slow asymptotic trend of Δ_{HL} toward the experimental energy gap of 3.2 eV (Ref. 32) is apparent as oligomers with 15 or more monomers increase in length.

The dependence on the oligomer chain length of both the radius of gyration R_g (average distance squared of monomers from the oligomer center of mass) and the end-to-end distance $d_{\text{end-end}}$ are depicted in Figs. 3(c) and 3(d). As expected based on the bent conformations shown in Fig. 2, the radius of gyration as a function of chain length [solid line in Fig. 3(c)] increases less rapidly than R_g of planar chains [dashed line in Fig. 3(c)]. Accordingly, the end-to-end distance is dramatically shorter [solid line in Fig. 3(d)] than that in planar chains [dashed line in Fig. 3(d)]. In the triplet state [triangles in Figs. 3(c) and 3(d)], both R_g and $d_{\text{end-end}}$ are closer to the planar chain values.

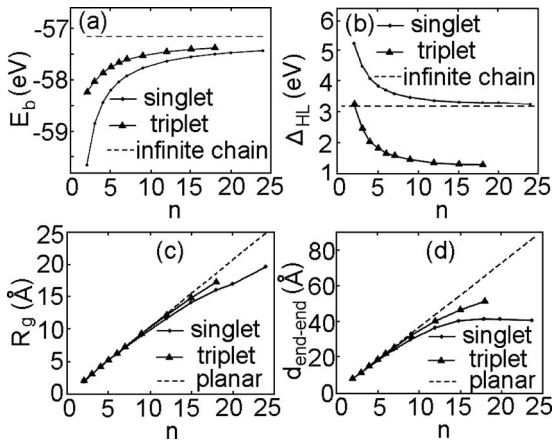

FIG. 3. Properties of reduced *n*-Py oligomers as a function of the number of monomers. (a) Binding energy per monomer, (b) HOMO-LUMO energy gap, (c) radius of gyration, and (d) end-to-end distance.

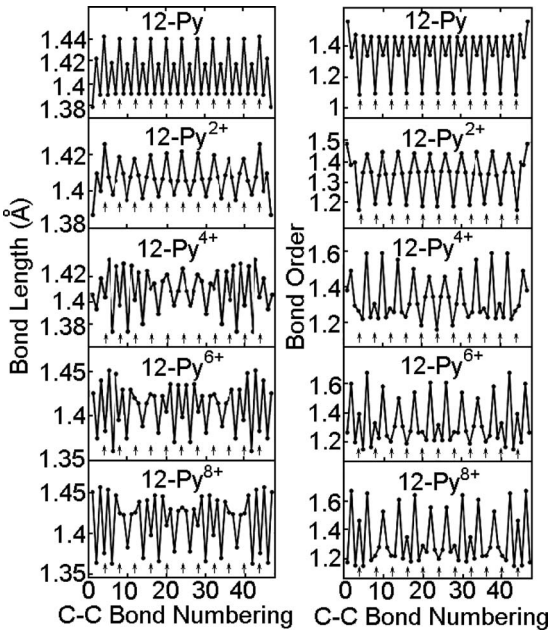

FIG. 4. Distribution of bond lengths and bond orders along the backbone of reduced and oxidized 12-Py. Arrows mark the position of the C—C inter-ring bonds.

The C—C bond length as a function of the C—C position in the 12-Py chain is depicted in the left top panel of Fig. 4 as an example of the oligomer benzenoid chains. The numbering of C—C bonds is sequential, starting with the double bond at one of the two chain ends. Arrows point to inter-ring C—C bonds. The Wiberg bond index[33,34] was calculated for the C—C bonds along the *n*-Py chain with results for 12-Py depicted in Fig. 4 (right top panel). There is a clear correlation between the bond length and bond order, reinforcing the expectation that intermonomer C—C single bonds are longer than the intramonomer C—C single bonds and have a substantially lower bond order. Additionally, the two end monomers in the oligomers display shorter C—C double bonds with higher bond orders.

The vibrational normal mode frequencies of the ground state and their IR-active intensities for *n*-Py ($n=3-6$, 9, and 12) are shown in the Appendix (Fig. 8). These spectra correspond to the equilibrium structures shown in Fig. 2. IR active frequencies of *n*-Py are predominantly distributed in two spectral regions: 700–1600 and 3000–4000 cm^{-1}. The far IR region is associated with motions involving several atoms in each ring, whereas most C—H and N—H stretching modes are in the near IR region. These vibrational spectra indicate that the two IR spectral regions are not sensitive to the size of the oligomer. Hence, reduced *n*-Py with different *n* have very similar vibrational spectra. As expected, the intensity of modes in these two spectral regions increases as the oligomer size increases.

IV. STRUCTURE AND ENERGETICS OF OXIDIZED *n*-Py OLIGOMERS

A thorough conformational optimization was implemented for positively charged *n*-Py oligomers as a function of the sustained positive charge Q. For these charged oligomers, ground states are doublets or singlets depending on Q being odd or even. The positive charge distributions for different degrees of oxidation are based on the Mulliken analysis of the geometry-optimized ground state wave function of each oligomer. For oxidized *n*-Py, the torsion angle is gradually increased from 153° as more positive charge Q is added to the backbone until the angle reaches 180° (planar chain) when the ratio $Q/n \geqslant 1/3$. For Q/n below 1/3, the *n*-Py oligomers may have out-of-plane structures with torsion angles other than 180° between them. Although not systematic, a study was carried out for these twisted oxidized *n*-Py configurations. Results indicate that out-of-plane backbones lead to oxidized *n*-Py isomers with high binding energies, which in several cases are saddles of the energy landscape.

The findings in this work show that high level oxidized *n*-Py ($Q/n \geqslant 1/3$) even-membered oligomers display a C_{2h} symmetry and odd-membered oligomers display a C_{2v} symmetry. However, low level oxidized oligomers ($Q/n < 1/3$) are bent with a smaller curvature than in neutral oligomers. For example 12-Py^{6+} and 12-Py^{4+} are planar with no puckering between the nearest neighbor rings, whereas in 12-Py^{2+} the torsion angle is increased from 153° (see Fig. 2) to 169°, as shown in Fig. 5. The effects of the increased oxidation level on the binding energy of oxidized oligomers (referred to the neutral) is summarized in Table IV (columns 6 and up). The effect of the increased oxidation level on the single/double C—C bond lengths and bond order structures is illustrated in Fig. 4. When *n*-Py is incipiently oxidized ($Q/n < 1/3$), the benzenoid conjugation of reduced *n*-Py is partly replaced with incipient trends of the quinoid structure. For example, in 12-Py^{2+} the benzenoid conjugation is still predominant, with inter-ring C—C single bonds being shorter and with C—C double bonds being expanded. However, as the ratio Q/n becomes $Q/n \geqslant 1/3$, then regions of quinoid alternation become clear. These quinoid regions span three monomers, as shown in Fig. 4 for 12-Py^{4+} and 12-Py^{6+}. Two of quinoid regions are visible in 12-Py^{4+}, indicating that the positive charge localized on each of these regions is $+2e$. In the case of 12-Py^{6+}, there are three quinoid regions, and again each region localizes a $+2e$ charge. If the charge is

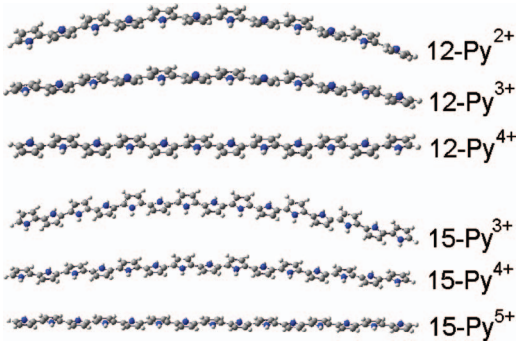

FIG. 5. (Color) Optimized structures of oxidized 12-Py^{m+} ($m=2$, 3, and 4) and 15-Py^{m+} ($m=3$, 4, and 5).

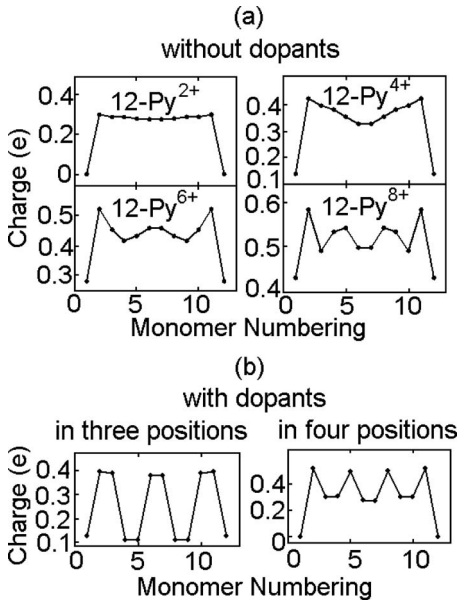

FIG. 6. Distribution of charge per monomer along the backbone of oxidized 12-Py. (a) Various oxidation levels and (b) charge localization due to dopants.

increased further as in 12-Py^{8+}, then the extent of the $+2e$ charge localization is shorter, barely covering two monomers. The energy of oxidized oligomers increases linearly by 0.92 eV/$(+e)$. The vibrational spectra of oxidized *n*-Py are similar to the neutral spectra, with the exception that frequencies in the 700–1600 cm^{-1} are two orders of magnitude more intense.

The conformational dependence on oxidation level findings is confirmed by analyzing the distribution of charge per monomer along the chain. Based on the Mulliken population analysis, the total charge on each monomer shows an increasing degree of localization in multiple regions of the chain as the oxidation level is increased. This effect is depicted in Fig. 6(a) showing two regions of localization in 12-Py^{4+}, three regions in 12-Py^{6+}, and four regions in 12-Py^{8+}. The charge localization takes place in multiples of $+2e$, which could be identified with the bipolaron.[17–19] Electron conduction then would take place by charge hopping between these localized regions.

Oxidation is attained experimentally with dopants. Typical oxidizing dopants include iodine, arsenic pentachloride, iron (III) chloride, and $NOPF_6$, which are electronegative compounds. A rough simulation of the effects of doping can be calculated within the hybrid DFT methodology used in this work by placing close to the chains high electron affinity atoms such as fluorine. The localization of positive charge will then take place around the positions where these electronegative atoms are located. In 12-Py, for example, if several F atoms are located symmetrically above and below the planar chain at three or four backbone positions where charge is peaked in Fig. 6(a), then oxidation takes place, yielding 12-Py^{+6} or 12-Py^{+8}. As shown in Fig. 6(b), negative charge is transferred from Py atoms at these backbone positions to the fluorine atoms.

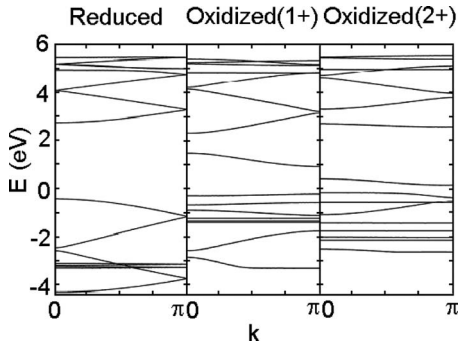

FIG. 7. Electronic band structure of infinite chains of reduced and oxidized PPy.

The oxidation level influences the HOMO-LUMO energy gap in *n*-Py. The calculated energy gap for reduced 12-Py is 3.36 eV, in agreement with the experimental[32] value of 3.2 eV for bulk PPy. Additionally, for every $+2e$ acquired by the oligomer upon oxidation, there is one localized state created in the gap. For 12-Py, upon oxidation the HOMO-LUMO gap decreases from 3.36 eV to 0.29, 0.73, 0.95, or 1.04 eV for every $+2e$ increase in the oxidation level. For oxidation levels where $Q/n<1/3$, the positive charge is delocalized along the backbone carbon atoms, and the new state created in the energy gap is close in energy to the HOMO. However, as oxidation reaches $Q/n=1/3$, charge localization occurs, and this effect results in level repulsion between the HOMO and the gap-localized states. For infinite PPy, these gap-localized states form a band, which may eventually overlap the valence band for the polymer to be conducting.

V. PPy INFINITE CHAIN

The electronic band structure of infinite chains was studied within the same hybrid DFT approach. For reduced PPy, a C_{2v} planar four-monomer chain was used in the unit cell of the periodic array. Figure 7 shows 16 bands around the Fermi energy, with all energies relative to the Fermi energy located at zero. Each band contains 80 *k*-points. The Fermi energy was determined as that energy for which the sum of the Fermi functions associated with each of the eigenvalues composing the bands was equal to the number of electrons. The energy band gap of the reduced PPy is 3.17 eV, which is in excellent agreement with the experimental value of 3.2 eV. Two oxidation levels of PPy were considered. For $+1e$ oxidation, the PPy was obtained by placing two F atoms 2.2 Å away from the center of a monomer in the unit cell, one above and one below. For $+2e$ oxidation, two F_2 dimers were placed in similar locations. The localized new band due to the charge is mainly an extended *p*-band formed by the carbon *p*-orbitals perpendicular to the plane of the monomers. The energy band gap shows a marked dependence with the oxidation level, decreasing from 1.78 eV for $+1e$ to 0.57 eV for $+2e$. Although fluorine is a strong electronegative element, because the dopants were placed far

away from the monomers, we did not fully attain a $+1e$ or $+2e$ charge transfer with either two F or two F_2, but rather $+1.08e$ and $+1.48e$ were obtained. For this reason, as seen in Fig. 7, the Fermi energy is still in the band gap and the valance band does not merge or cross the new localized band as expected in a conductor material. Increasing the basis set size to include diffuse *d*-functions does not change significantly the band structure shown in Fig. 7.

VI. CONCLUSION

In summary, this is an exhaustive set of structural and energetic results for *n*-Py oligomers ($n=1-24$) in both the reduced and oxidized phases. Outstanding features of the reduced oligomers are their notoriously bent spatial conformations, which result in strong reductions in their radius of gyration and end-to-end distance as compared to planar oligomers. As a result of oxidation (charge Q), these oligomers become increasingly planar until the critical value of $Q/n=1/3$ yields an oxidation level in which the oligomers are planar. This critical oxidation level is also accompanied by a spatial localization of positive charge, which is usually referred to as a polaron. Below the critical value, the oxidized oligomers present a delocalized positive charge distributed along the oligomer backbone C atoms. The vibrational spectra of *n*-Py oligomers display two fairly size-insensitive IR spectral regions at 700–1600 and 3000–4000 cm^{-1}, which only change slightly with oxidation. As expected, if in the proximity of *n*-Py several electronegative dopants are included in the calculation, Q localizes in the neighborhood of the dopant and one localized state in the HOMO-LUMO gap appears for every $+2e$ in the oxidation level. The energy band gap of infinite PPy is in excellent agreement with experiment. Additionally, the trend of a decreasing band gap with increasing oxidation level is clearly demonstrated.

Altogether, this study provides a comprehensive and complete compendium of the effects that reduction-oxidation changes produce in the electronic structure, conformation, energetics, and vibrational spectra on *n*-Py and infinite PPy chains.

ACKNOWLEDGMENTS

The National Institute of Standards and Technology Cooperative Agreement No. 70NANB5H1110 is acknowledged for partial support allocated to Y.D.'s graduate assistantship. The Teragrid grant (No. PHY050023T) is acknowledged for computing time in the SMP platform at the Pittsburgh Supercomputing Center. We are thankful to Professor E. Smela for useful discussions and for bringing to our attention her experimental work on PPy.

APPENDIX: VIBRATIONAL ANALYSIS

The vibrational normal mode frequencies of the ground state and their IR-active intensities for *n*-Py ($n=3-6$, 9, and 12) are shown in Fig. 8.

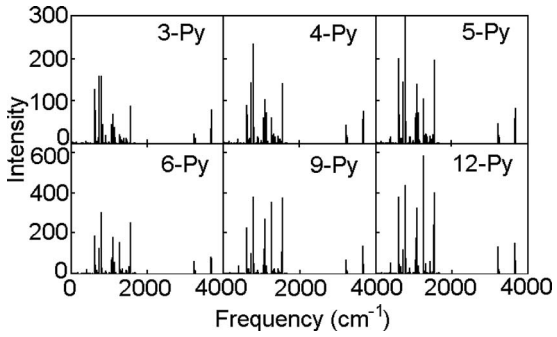

FIG. 8. IR-active vibrational spectra of reduced *n*-Py ($n=3$, 4, 5, 6, 9, and 12).

[1] E. Smela, J. Micromech. Microeng. **9**, 1 (1999).
[2] E. Smela and N. Gadegaard, Adv. Mater. (Weinheim, Ger.) **11**, 953 (1999).
[3] W. K. Ford, C. B. Duke, and W. R. Salaneck, J. Chem. Phys. **77**, 5030 (1982).
[4] B. Tian and G. Zerbi, J. Chem. Phys. **92**, 3886 (1990).
[5] B. F. G. I. Ivanov and D. Yaron, Synth. Met. **116**, 111 (2001).
[6] D. Beljonne and J. L. Bredas, Phys. Rev. B **50**, 2841 (1994).
[7] J. L. Bredas, B. Themans, J. G. Fripiat, and J. M. Andre, Phys. Rev. B **29**, 6761 (1984).
[8] J. M. Andre, D. P. Vercauteren, G. B. Street, and J. L. Bredas, J. Chem. Phys. **80**, 5643 (1984).
[9] X. Lin, J. Li, E. Smela, and S. Yip, Int. J. Quantum Chem. **102**, 980 (2005).
[10] J. L. Bredas, G. B. Street, B. Themans, and J. M. Andre, J. Chem. Phys. **83**, 1323 (1985).
[11] M. Kofranek, T. Kovar, A. Karpfen, and H. Lischka, J. Chem. Phys. **96**, 4464 (1992).
[12] I. Rabias and B. J. Howlin, Comput. Theor. Polym. Sci. **11**, 241 (2001).
[13] U. Salzner, P. G. Pickup, R. A. Poirier, and J. B. Lagowski, J. Phys. Chem. A **102**, 2572 (1998).
[14] R. Colle and A. Curioni, J. Am. Chem. Soc. **120**, 4832 (1998).
[15] R. Burcl, R. D. Amos, and N. C. Handy, Chem. Phys. Lett. **355**, 8 (2002).
[16] S. Y. Lee and B. H. Boo, J. Phys. Chem. **100**, 15073 (1996).
[17] J. L. Bredas, R. R. Chance, and R. Silbey, Mol. Cryst. Liq. Cryst. **77**, 319 (1981).
[18] J. L. Bredas, R. R. Chance, and R. Silbey, Phys. Rev. B **26**, 5843 (1982).
[19] R. R. Chance, J. L. Bredas, and R. Silbey, Phys. Rev. B **29**, 4491 (1984).
[20] J. P. Perdew, J. A. Chevary, S. H. Vosko, K. A. Jackson, M. R. Pederson, D. J. Singh, and C. Fiolhais, Phys. Rev. B **46**, 6671 (1992).
[21] J. P. Perdew, K. Burke, and Y. Wang, Phys. Rev. B **54**, 16533 (1996).
[22] R. S. R. Krishnan, J. S. Binkley, and J. A. Pople, J. Chem. Phys. **72**, 650 (1980).
[23] M. J. Frisch, G. W. Trucks, H. B. Schlegel *et al.*, GAUSSIAN 03, Revision C.01, Gaussian, Inc., Wallingford, CT, 2004.
[24] L. Nygaard, J. T. Nielsen, J. Kirchheiner, G. Maltesen, J. Rastrup-Andersen, and G. O. Sorensen, J. Mol. Struct. **3**, 491 (1969).
[25] R. Navarro and J. Orza, An. Quim. Ser. A **79**, 557 (1983).
[26] *Handbook of Conducting Polymers*, edited by T. A. Skotbeim (Deckker, New York, 1986).
[27] Y. Dai, Ph.D. thesis, George Mason University, Fall semester 2008.
[28] H. B. S. C. Peng, P. Y. Ayala, and M. J. Frisch, J. Comput. Chem. **17**, 49 (1996).
[29] R. Kaner and A. G. MacDiarmid, Sci. Am. **258**(2), 106 (1988).
[30] A. G. MacDiarmid, Synth. Met. **84**, 27 (1997).
[31] G. Zotti, S. Martina, G. Wegner, and A. D. Schluter, Adv. Mater. (Weinheim, Ger.) **4**, 798 (1992).
[32] G. Street, T. C. Clarke, M. Krounbi, K. K. Kanazawa, V. Y. Lee, P. Pfiuger, J. C. Scott, and G. Weiser, Mol. Cryst. Liq. Cryst. **83**, 253 (1982).
[33] I. Wiberg, Chem. Phys. Lett. **97**, 270 (1983).
[34] F. Weinhold and J. E. Carpenter, in *The Structure of Small Molecules and Ions*, edited by R. Naaman and Z. Vager (Plenum, New York, 1988).